ELSEVIER

Journal of Nuclear Materials 289 (2001) 315–328

journal of nuclear materials

www.elsevier.nl/locate/jnucmat

Pre-transition oxidation behaviour of pre-hydrided Zircaloy-2

M. Oskarsson [a], E. Ahlberg [b,*], U. Södervall [c], U. Andersson [b], K. Pettersson [a]

[a] *Department of Materials Science and Engineering, Royal Institute of Technology, SE-10044 Stockholm, Sweden*
[b] *Department of Chemistry, University of Göteborg, SE-41296 Göteborg, Sweden*
[c] *Department of Microelectronics and Nanoscience, Chalmers University of Technology, SE-41296 Göteborg, Sweden*

Received 15 August 2000; accepted 4 December 2000

Abstract

Oxidation tests with hydrogen present in three different states were performed: (i) Hydrogen in solid solution in the zirconium alloy, corresponding to the initial oxidation prior to precipitation of hydrides. (ii) Uniformly distributed hydrides, simulating a situation where hydrides start to precipitate and (iii) massive surface hydride, claimed to be the main cause of accelerated oxidation. The pre-hydrided samples and a reference (REF) sample were oxidised in steam in a static autoclave at 400°C and 10 MPa for 3, 10 and 25 days. The oxide formed was characterised by X-ray diffraction (XRD), transmission electron microscopy (TEM), secondary ion mass spectrometry (SIMS) and electrochemical impedance spectroscopy (EIS). Based on the results obtained, it is concluded that the oxidation of massive zirconium hydride resembles the oxidation of zirconium metal. This fact shows that the commonly observed accelerated oxidation of zirconium alloys cannot be due to an increased oxidation rate of the hydride compared to the metal,but must require a combined effect of, for example interfacial roughness and hydride precipitation. The results are discussed in relation to the mechanism of corrosion and hydriding of zirconium alloys.

1. Introduction

During oxidation of zirconium and its alloys in aqueous environment hydrogen is released from the water molecule. A fraction of the hydrogen formed is absorbed by the metal during the corrosion process and when the terminal solubility limit is reached hydrides precipitate. The mechanical properties of Zircaloy are degraded when hydrides are present in the metal.

High levels of hydrogen are often found in samples that have been subjected to an accelerated corrosion rate and the key question is whether the high hydrogen levels are a cause or a consequence of the accelerated oxidation kinetics. To answer this question it is necessary to compare the oxidation behaviour of the alloy, pre-hydrided samples with hydrogen in solid solution, uniformly distributed hydrides and samples with a massive surface hydride.

Many studies have been performed on purpose to evaluate the behaviour of hydrogen in zirconium alloys and how the oxidation is affected. The terminal solid solubility (TSS) for hydrogen in Zircaloy-2 (Zr-2) is ~200 ppm at 400°C [1], and at higher hydrogen levels hydrides will be present. Addition of oxygen will increase the TSS for hydrogen and this has been suggested to be an effect of an increase in the matrix strength or hydrogen trapping at the solute atoms [2]. However, at high concentrations of oxygen the hydrogen solubility will decrease [3]. At higher temperature, 600–775°C, the solubility increases with oxygen content, but then decreases when the O/Zr ratio is above 0.177 [4]. Oxygen is found in octahedral and hydrogen in tetrahedral positions in zirconium. It is thermodynamically more favourable for the oxygen to be in solid solution in the metal, but the kinetics do not allow the oxygen to diffuse a long distance from the oxide/metal interface at the studied temperature, so an oxide will form. The solubility for hydrogen in the oxide films is low [5] and decreases with increasing temperature [6].

It was early discovered that nickel increases the hydrogen absorption. The hydrogen absorption during

* Corresponding author. Tel.: +46-31 772 2879; fax: +46-31 772 2853.
E-mail address: ela@inoc.chalmers.se (E. Ahlberg).

0022-3115/01/$ - see front matter
PII: S0022-3115(01)00416-0

corrosion was studied for Zr-2 and some binary alloys in water at 316–400°C [7]. Comparing the Zr-2 alloy with different binary alloys the authors report that tin has little or no effect, iron and chromium decrease, while nickel aids the hydrogen ingress through the oxide layer [7].

The transport mechanism of hydrogen through the oxide layer is not fully understood but different hypotheses have been proposed to explain the ingress of hydrogen. The early models suggest diffusion of hydrogen through the oxide layer in different ways:

(i) The hydrogen ingress occurs by proton hopping from O^{2-} to O^{2-} in the oxide, towards the metal [8]. Also diffusion of OH^- was discussed, but was disregarded by the authors because only one proton per oxygen atom could enter and the maximum hydrogen uptake should be less than 50%. However, this argument is not valid since during corrosion tests at normal conditions the hydrogen uptake is always less than 50%.

(ii) Diffusion of hydrogen atoms through the oxide layer via anion vacancies. Here the generation of anion vacancies are believed to take place at the metal/oxide interface when oxygen jumps to an interstitial position in the metal [9]. Another possibility is ingress through easy diffusion paths such as dislocation lines and grain boundaries [10].

However, nowadays the diffusion of hydrogen through a compact oxide is regarded as less plausible. The main ingress routes considered today are through defect oxide layers [11–14] and non-oxidised second phase particles (spp) within the protective oxide film [15–17]. For example, transmission electron microscopy (TEM) investigations of thin oxide films formed on pure zirconium (400°C for 24 h) have shown that an interconnected network of pores may form, following the equiaxed grain boundaries and the hydrogen permeation may take place via this pore network [12]. In the newer models the hydrogen ingress is regarded as a localised process and it is suggested that a microscopic steam process is taking place in small cracks, leading to an accumulation of hydrogen close to the oxide/metal interface. The passive oxide at the bottom of the crack is thought to break down during this process and hydrogen enters the metal [14]. In the cited experiments the oxidation test was performed on thin Zr-2 plates in steam at 300–400°C. When the TSS was reached, which occurred during the pre-transition oxidation, the uptake rate of hydrogen decreased.

Corrosion tests on pre-hydrided Zr-4 at 360°C showed that the corrosion rate increased with increasing initial hydrogen content [18], and it is hypothesised that the hydrogen present in the metal close to the oxide/metal interface enhances the corrosion. The cause of the accelerated oxidation rate in the presence of high hydrogen levels and/or hydrides has been discussed in the literature. The accelerated corrosion rate at long times is proposed to be a consequence of the fracture of the precipitated hydrides at the metal/oxide interface [19]. Another hypothesis proposes that the properties of the oxide may be modified when the oxide grows on massive hydrides or on metal with high hydrogen content [20]. Hydrogen may change the transport mechanism and/or the morphology of the growing oxide. However, more recently the effect of hydrogen on the oxidation behaviour of Zr-4 was investigated by the same authors and no significant changes in morphology were detected by TEM examination of the oxide layer [21]. A difference in the density of cracks was observed, being higher in the oxide formed on massive hydride layers, and an enrichment of hydrogen in the inner part of the post-transition oxide was detected by SIMS on pre-hydrided material. The effect of the pre-hydriding process itself on the oxidation behaviour was also evaluated in this study [21], but no influence was found.

In the present work pre-hydrided Zr-2 was subjected to corrosion testing in a static autoclave. To get a good comprehensive view of the effect of hydrogen on the oxidation process different analysis techniques have been utilised. The composition of the oxide layers was characterised by X-ray diffraction (XRD) while cross-sectional TEM investigation gives information about the oxide morphology, thickness of the oxide film and microstructure of the oxide, such as cracks and precipitates. However, the sample preparation technique influences the oxide crystal structure and the presence of cracks [22]. Electrochemical impedance spectroscopy (EIS) investigations give information on the open porosity and total porosity in the oxide layer. The electrical properties and the thickness of the oxide layer can also be evaluated. Based on this result the passivating properties of the oxide can be judged. By secondary ion mass spectrometry (SIMS) the element profile in the oxide and metal can be traced and it is possible to study the distribution of hydrogen in the material.

2. Experimental

The material under investigation was standard Zr-2 tubes, manufactured by Sandvik Steel AB. It is fully crystallised with a final annealing temperature of 565°C ($\log A = -15.4$ calculated with $Q = 63\,000$ cal/mol). The material has small (average diameter 80 nm) spp and the chemical composition is given in Table 1.

The hydrides were produced by gas hydrogenation. Before exposure to hydrogen gas the samples were treated in high vacuum for 24 h at room temperature, 0.5 h at 200°C and 0.5 h at 400°C, in order to condition the samples for hydrogen up-take. Then the samples were heated for 0.5 h at 400°C with hydrogen gas added to obtain the predetermined hydrogen level. The amount

Table 1
Chemical composition of Zircaloy-2

Sn (wt%)	Fe (wt%)	Cr (wt%)	Ni (wt%)	
1.28	0.182	0.104	0.06	
O (ppm)	Si (ppm)	C (ppm)	H (ppm)	N (ppm)
1250	92	108	5	32.5

of absorbed hydrogen was measured by pressure decrease in a known volume and by measuring the weight gain after performed hydriding. Two samples with 200 ppm and two with 500 ppm hydrogen were produced. For each level one sample was heat-treated (HT) after hydrogenation, for 24 h at 550°C, to get uniformly distributed hydrides. These samples were investigated by scanning electron microscopy (SEM) to see if the microstructure was affected by the heat treatment. No changes were observed. The hydrided samples show the same metal lustre after hydrogenation as before and it can therefore be concluded that no oxidation occurred during the pre-hydriding process. The hydride structure of the four samples was investigated by light optical microscopy (LOM) and the micrographs are given in Fig. 1.

One reference (REF) sample and the pre-hydrided samples were oxidised in steam in a static autoclave at 400°C and 10 MPa for 3, 10 and 25 days. LOM examination of the hydride structure showed no discernible changes in distribution of the hydrides after oxidation.

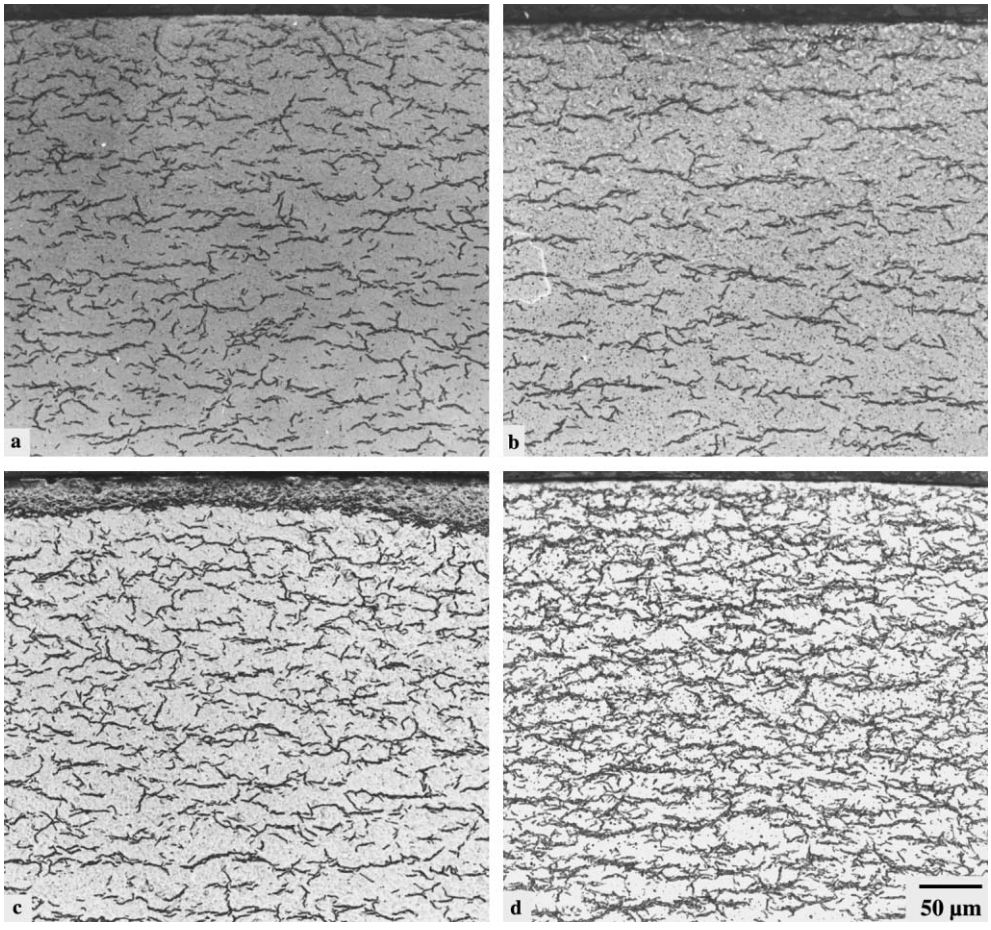

Fig. 1. Light optical micrograph of cross-section of the pre-hydrided samples: (a) 200 ppm H, with surface hydride sample (I); (b) 200 ppm H heat-treated (II); (c) 500 ppm H, with surface hydride (III); (d) 500 ppm H heat-treated (IV).

2.1. XRD

A Siemens D5000 powder diffractometer equipped with grazing incidence beam attachment and a Göbel mirror were used to characterise the non-oxidised samples. CuK_α radiation was used and the angle of incidence was 0.50°. The grazing incidence of the beam allowed for characterisation of thin surface layers. For the oxidised samples the measurements were made at 0.018° intervals of 2θ over the range 20–70° with a count-time of 20 s at each angle.

2.2. TEM

To characterise the microstructure of the oxide layers for the autoclaved samples, cross-sectional thin foils were produced. Preparation of the foils was done by gluing the oxidised tube to a stainless steel tube (ss), with $d^{ss}_{inner} > d^{Zr}_{outer}$, and a small piece was then cut from the 'composite tube'. The piece was put inside a brass tube (3 mm outer diameter) and an epoxy/carbon mix was added to keep the piece in position. From the brass tube a slice was cut perpendicular to the oxide surfaces and mechanically thinned to approximately 35 μm. The last step of the sample preparation was ion etching in a Gatan precision ion polishing system (PIPs) with argon ions at 5.0 kV. The ion etching continued until a hole was developed and the examination was made at the electron transparent edges of the hole. The oxide layers were characterised in a JEOL 2000 EX scanning TEM.

2.3. EIS

Two different types of impedance measurements were conducted. A two-electrode system was used to measure the resistance and the capacitance of the non-wetted oxide films. The electrode sample was immersed in mercury, which acts as the counter electrode in these experiments. A three-electrode cell was used for the impedance experiments in aqueous 0.5 M Na_2SO_4. A platinum gauze was used as the counter electrode and the potential was measured against a double junction Ag/AgCl REF electrode with 0.5 M Na_2SO_4 in the outer compartment. A one centimetre sample of the Zircaloy tube acts as the working electrode, exposing only the oxidised surface to the electrolyte. The electrolyte was made from p.a. quality chemicals and doubly distilled water and was used without de-gassing the solution. All impedance measurements were carried out at room temperature under stationary conditions, in the frequency range 0.001 Hz–100 kHz. The instrumentation used was an EG & G Princeton Applied Research Potentiostat/Galvanostat Model 273A, and a Schlumberger SI 1255 HF frequency response analyser.

The impedance data were fitted using an equivalent circuit with one or more time constants. The impedance data exhibit some frequency dispersion and a constant phase element was used instead of a capacitor.

2.4. SIMS

The hydrogen distribution through oxide and into the metal was analysed by means of SIMS in-depth profiling. A CAMECA-IMS 6f instrument was used. Positive cesium ions were used for sputtering with a primary ion current of 50–100 nA and a beam diameter of 25 μm. The primary beam was rastered over an area of 200×200 μm^2, while secondary ions were only detected from the central 60 μm diameter area. The depth scale was calibrated by measuring the crater depth with a surface profilometer, Talysurf-10. Besides secondary ions of H^- also C^-, O^-, F^-, Zr^-, Zr_2^- and alloying elements were analysed in each depth profile. The H signal was normalised to the Zr-signal to reduce the matrix effects. We have observed a difference in the sputter rate of the oxide and the metal of about 50% (faster in metal). The absolute level of hydrogen in the metal was calibrated using the known level in pre-hydrided samples with a uniform distribution. The same sensitivity factor was used for hydrogen in the oxide, resulting in a background level for H detection of approximately 2 ppm both in the oxide and the metal. For some of the profiles a different sputtering rate was used, which increases the detection limit for hydrogen to 10 ppm in the oxide.

3. Results

From the weight gain data the thickness of the oxide layers has been calculated and the results are given in Table 2. These data can be compared with the oxide thickness measured with TEM and EIS. The agreement between the different techniques is reasonably good.

3.1. XRD analysis

The four pre-hydrided samples were investigated with grazing angle XRD analysis, Fig. 2. For the HT samples (II and IV) only the diffraction peaks for zirconium metal can be observed, showing that the hydrides are absent in the surface. The standard reflections for zirconium metal are added in the figure of sample II and it can be seen that the (1 0 0) reflection is reduced while the (0 0 2) reflection is favoured, due to texture in the metal phase.

For sample III with a massive surface hydride layer, the diffractogram shows the presence of δ-ZrH_2. Due to the rather thick layer of hydride, see Fig. 1, only small diffraction peaks for zirconium metal are observed. The standard reflections for δ-ZrH_2 are also given in the figure. For sample I, the surface hydride was not clearly

Table 2
Oxide thickness (μm) calculated from weight gain (WG) and measured by TEM, EIS and SIMS

Sample	Hydrogen content (ppm)	3 days				10 days				25 days			
		WG	TEM	EIS	SIMS	WG	TEM	EIS	SIMS	WG	TEM	EIS	SIMS
REF	5	1.0				1.4	1.3	1.5	1.4	1.7			
I	200 Surface hydride	1.1				1.5	1.5	2.1	2.2	1.9			
II	200 HT	1.2	1.25		1.25	1.6	1.6	1.5	1.6	2.4	2.5	2.5	2.5
III	500 Surface hydride	1.0				1.5	1.7	1.7	1.3	2.0			
IV	500 HT	1.0				1.6	1.7	1.4	2.0	–*			

* Experimental failure, no data available.

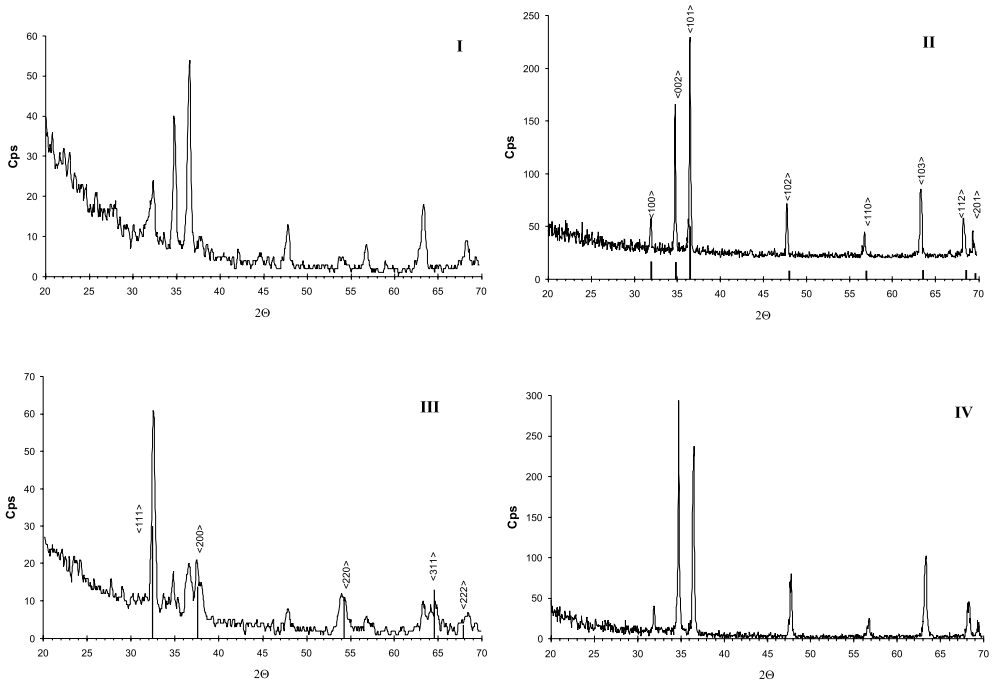

Fig. 2. Grazing angle XRD of the pre-hydrided samples. The standard reflections for Zr are given in II and for δ-ZrH_2 in III.

visible in the LOM, but a surface hydride is clearly seen in the diffractogram. Also in this case the δ-ZrH_2 was formed. In this case the diffraction peaks for zirconium metal are more pronounced since the surface hydride layer is thinner. For a previously oxidised sample (III) an additional experiment was performed to ensure that the surface hydride remains during the 400°C oxidation testing. XRD spectra were measured in air at 400°C for 18 h and no changes in the reflections for the hydride were observed as a function of time.

After oxidation the samples were again subjected to X-ray analysis in order to determine the composition of the surface layer. The diffractograms for the four pre-hydrided samples, oxidised for 10 days, are shown in Fig. 3. The data are normalised by the intensity of the Zr reflection at $2\theta = 34.84°$. The oxide film on all samples consists of mainly monoclinic ZrO_2 but with a detectable amount of the tetragonal phase, as shown by the inserted standard reflections for the m-ZrO_2 and t-ZrO_2, respectively. For sample III it is clearly seen that the existence of a massive hydride layer has not changed the composition of the oxide and further, the hydride signal is readily observed. When the variable angle mode is used (as for the oxidised samples) a larger penetration depth is traced than for the grazing angle mode, and therefore the reflections from the metal are more pronounced than for the non-oxidised samples (compare with Fig. 2). For the same reason, the hydride signal is not observed for the oxidised sample I. For the monoclinic oxide some preferential orientation effects are

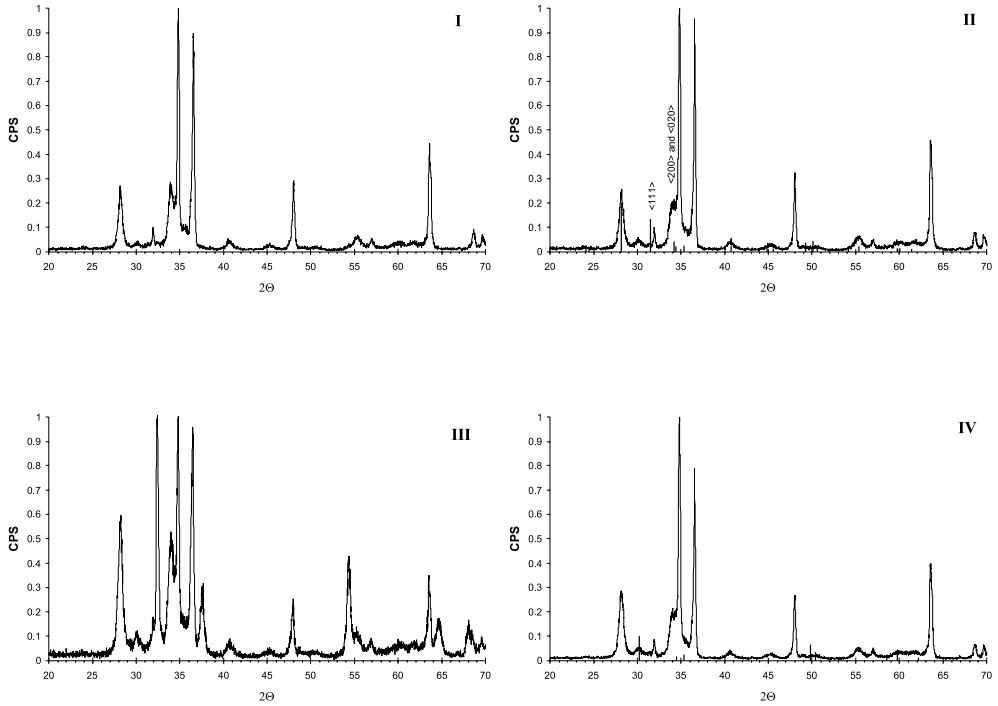

Fig. 3. XRD of the pre-hydrided samples after 10 days of oxidation. The standard reflections for m-ZrO_2 and t-ZrO_2 are given in II and IV, respectively. The signal has been normalised by the intensity of the reflection at $2\theta = 34.84°$.

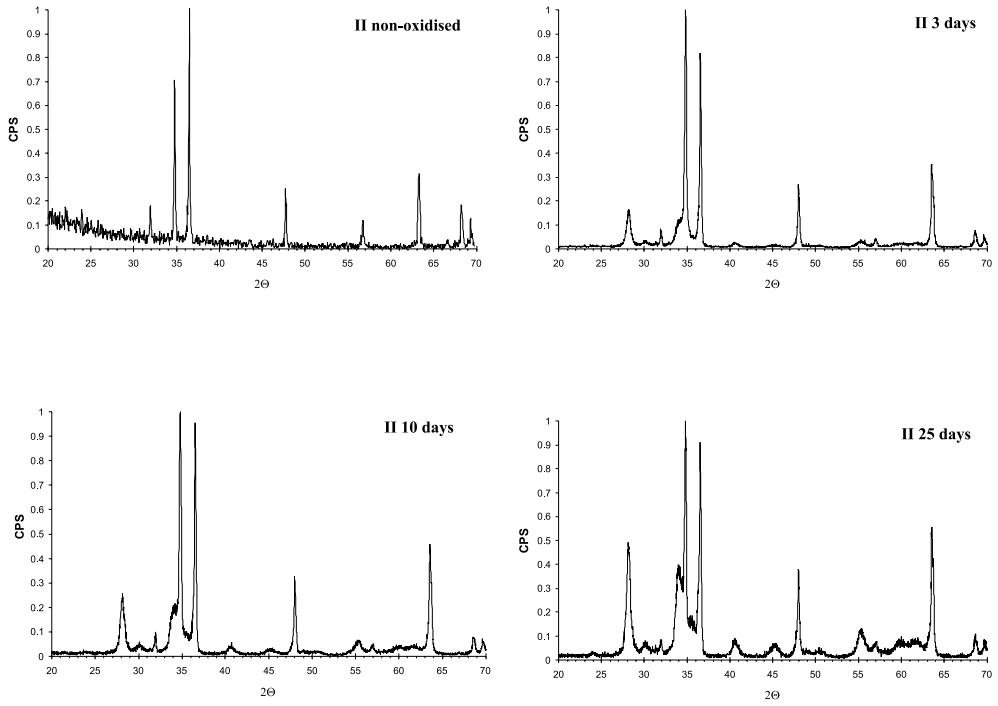

Fig. 4. XRD of sample II after 0, 3, 10 and 25 days oxidation. The signal has been normalised by the intensity of the reflection at $2\theta = 34.84°$.

observed. For example, the (1 1 1) reflection at $2\theta = 31.5°$ is absent while the reflections at 34.16 (2 0 0) and 34.83 (0 2 0) are more pronounced than expected from random orientation of crystallites. For the tetragonal oxide only the strongest reflection is observable due to the small amount of oxide present. The ratio between the monoclinic and tetragonal oxide phases is not affected by the hydrogen level in the metal and is also the same for different thicknesses of the oxide scale. This is illustrated in Fig. 4, where normalised diffractograms for sample II are shown. Although the oxide thickness increases, as can be seen from the relative increase of the oxide reflections compared to the metal reflections with increasing oxidation time, the ratio between the reflection at 30.2° (t-ZrO_2) and 28.2° (m-ZrO_2) remains the same.

From the results of the XRD data the oxide films formed on the different samples seem to be very similar, irrespective of whether it is grown on a massive zirconium hydride or on zirconium metal.

3.2. TEM

For all investigated samples the oxide layer has a morphology with mainly columnar grains but also a small fraction of equiaxed grains. A representative TEM micrograph is shown in Fig. 5. The micrograph is from the 200 ppm hydrogen sample (I) oxidised for 10 days. The sizes of the columnar grains are $(20–35) \times (100–200)$ nm and the equiaxed grains are 15–30 nm in diameter. The growth direction of the columnar grains is perpendicular to the interface. All oxide layers also have cracks present with an orientation parallel to the oxide/metal interface. The oxide grains present at these cracks are mainly equiaxed, in agreement with earlier studies [22,23].

The HT samples with 200 ppm hydrogen (II) were analysed after 3, 10 and 25 days of oxidation. Beside the thickness no major difference in morphology was found. The sample with 500 ppm hydrogen (III) containing a massive surface hydride layer has, after 10 days of oxidation, an oxide layer with columnar and equiaxed grains as shown in Fig. 6(a). On this sample the fraction of columnar grains is somewhat less than on the samples with lower initial hydrogen content. However, a majority of the grains are still columnar. The oxide layer formed after 10 days of oxidation for the heat-treated sample with 500 ppm hydrogen (IV), with a uniform hydride distribution, has a morphology similar to the sample with massive surface hydride, see Fig. 6(b).

3.3. EIS

The impedance spectra for the oxidised samples (10 days) are shown in Fig. 7. For all samples the impedance spectra obtained in mercury show only one time

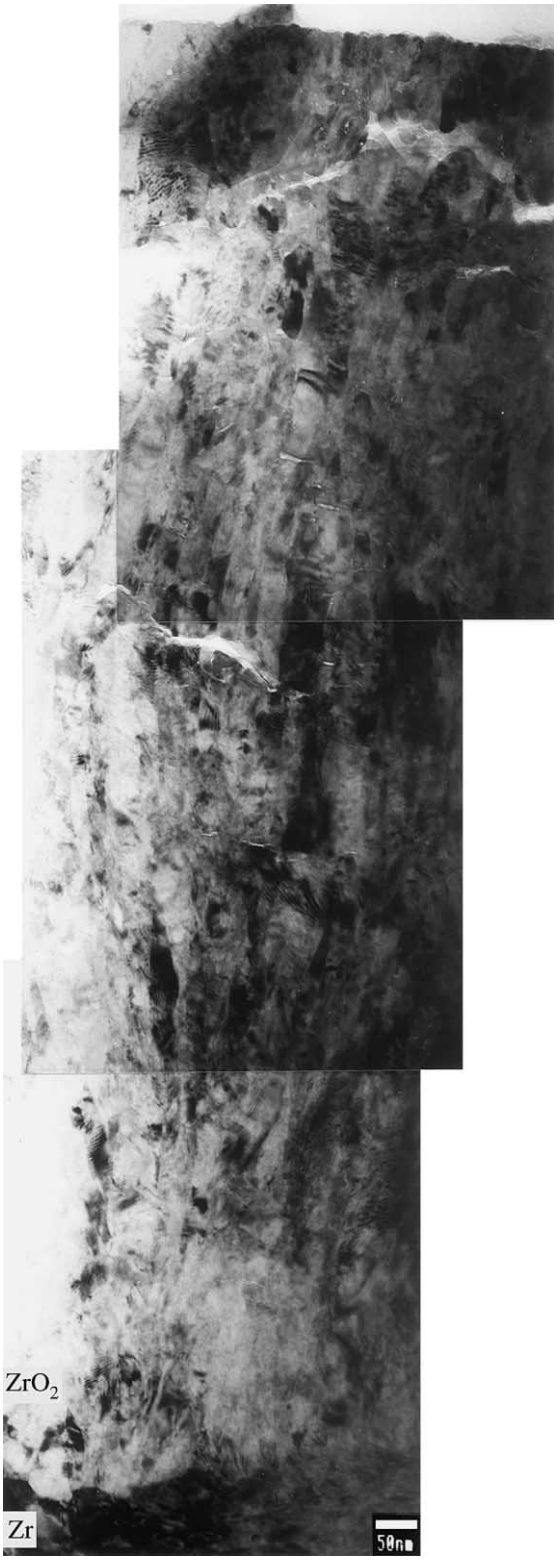

Fig. 5. TEM micrograph showing sample I after 10 days oxidation.

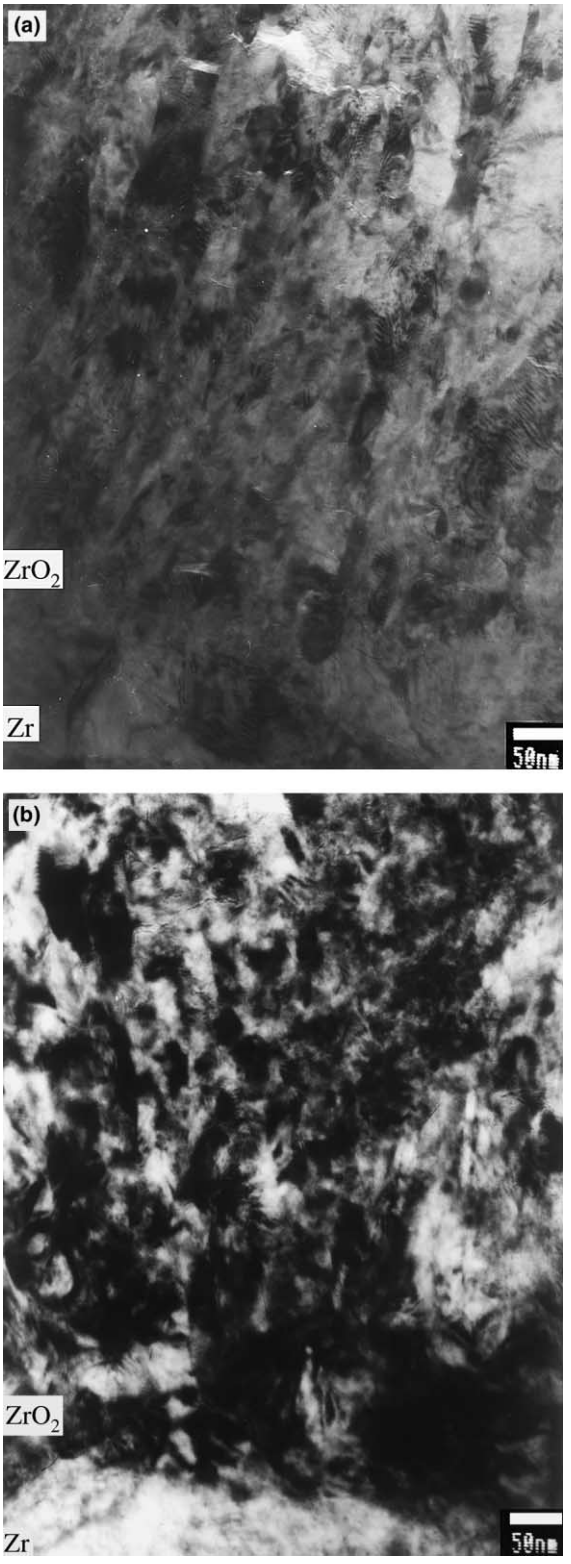

Fig. 6. TEM micrograph of two samples after 10 days oxidation: (a) Sample III; (b) Sample IV.

constant. The resistance of the oxide is high in all cases, but for the HT samples (II and IV) a decrease in the order of one magnitude can be observed. In aqueous electrolyte, impedance spectra were recorded as a function of time until no further changes were observed. The highly conducting electrolyte will penetrate into the open pores and lower the resistance over the oxide. The impedance characteristics of well-soaked samples will also give a qualitative information on the pore texture of the oxide layer. The presence of two or more time constants indicates that the properties of the oxide layer changes with distance from the metal/oxide interface. The different time constants can for example be due to a layered oxide structure with different pore sizes and distributions. In Fig. 7 the final impedance spectra show that for the REF sample and the samples containing a surface hydride (I and III), only one time constant is observed, indicating that these oxides are homogeneous. However, for the HT samples two time constants were necessary in order to fit the experimental data and thus from the impedance data somewhat more inhomogeneous oxide films are expected.

Zirconium oxide is highly insulating and the overall impedance can therefore be attributed to the impedance of the oxide. The oxide behaves like a capacitor in the impedance measurements and the capacitance is given by the expression for a parallel plate capacitor,

$$C = \frac{\varepsilon_0 \varepsilon_r A}{d}, \tag{1}$$

where ε_0 is the dielectric constant of vacuum, ε_r is the relative dielectric constant for ZrO_2, A is the geometric surface area, d is the thickness of the oxide layer and C is the capacitance.

The total porosity of the oxide layer formed during the autoclave experiments was measured by immersion of the sample in mercury. Mercury with its high surface tension will not penetrate into the pores of the oxide, and therefore the impedance of the entire oxide can be measured. If the oxide is massive the thickness can be calculated according to Eq. (1), using a value of 22 for the relative dielectric constant for ZrO_2 [24,25]. However, if the oxide contains pores, these will be filled by air and the relative dielectric constant of the oxide scale (ε_{app}) will depend on the total porosity. Assuming that x is the fraction of pores in the oxide, the apparent relative dielectric constant can be written

$$\varepsilon_{app}^{-1} = x\varepsilon_{air}^{-1} + (1-x)\varepsilon_{ZrO_2}^{-1}. \tag{2}$$

If the thickness of the oxide is known the total porosity of the oxide layer can thus be evaluated. In the present work the thickness of the oxide layer was calculated from the weight gain experiments and the resulting porosity is given in Table 3.

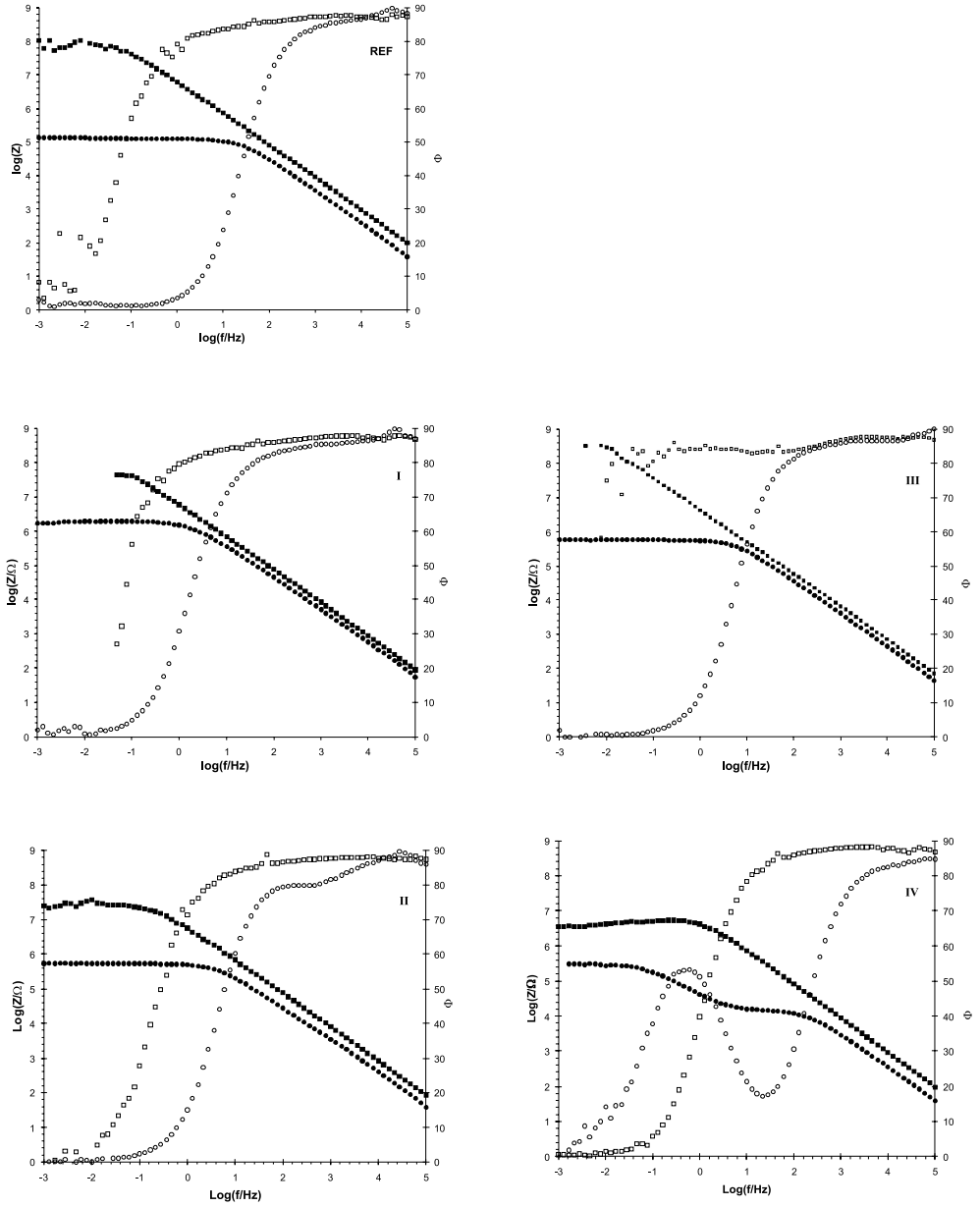

Fig. 7. EIS investigation of the pre-hydrided samples after 10 days of oxidation. Measurements in mercury (■) magnitude and (□) phase angle. Measurements in 0.5 M Na_2SO_4 (●) magnitude and (○) phase angle.

Table 3
Total porosity measured with impedance

Sample	Porosity (%)
REF, 10 days	6.1
I, 10 days	5.6
II, 3 days	4.2
II, 10 days	4.5
II, 25 days	4.8
III, 10 days	3.7
IV, 10 days	5.7

In aqueous electrolyte the open pores will be filled with electrolyte. Since the relative dielectric constant of water is large ($\sim$80) the apparent relative dielectric constant of the oxide layer will be close to the value for the oxide itself. Thus, the thickness of the oxide layer can be calculated according to Eq. (1) and good agreement with the value obtained by weight gain and TEM was observed, Table 2. For the calculation of oxide thickness the capacitance obtained at the highest frequencies was used.

In Fig. 8 the impedance spectra for sample II, oxidised at 400°C for 25 days, are shown. The impedance indicates that the oxide layer formed in the oxidation process is somewhat porous, with changes in the pore texture traversing from the metal/oxide to the oxide/solution interface, giving rise to several time constant. However, the fact that the entire oxide thickness is measurable with impedance shows that the oxide layer is relatively dense. In comparison with the impedance spectra obtained on samples with shorter oxidation time, the oxide seems to be more inhomogeneous. This fact, however, does not necessarily mean that the morphology of the oxide has changed. This is clearly seen by the TEM micrograph of the same sample, Fig. 8(a), showing that the morphology resembles that obtained for shorter oxidation times.

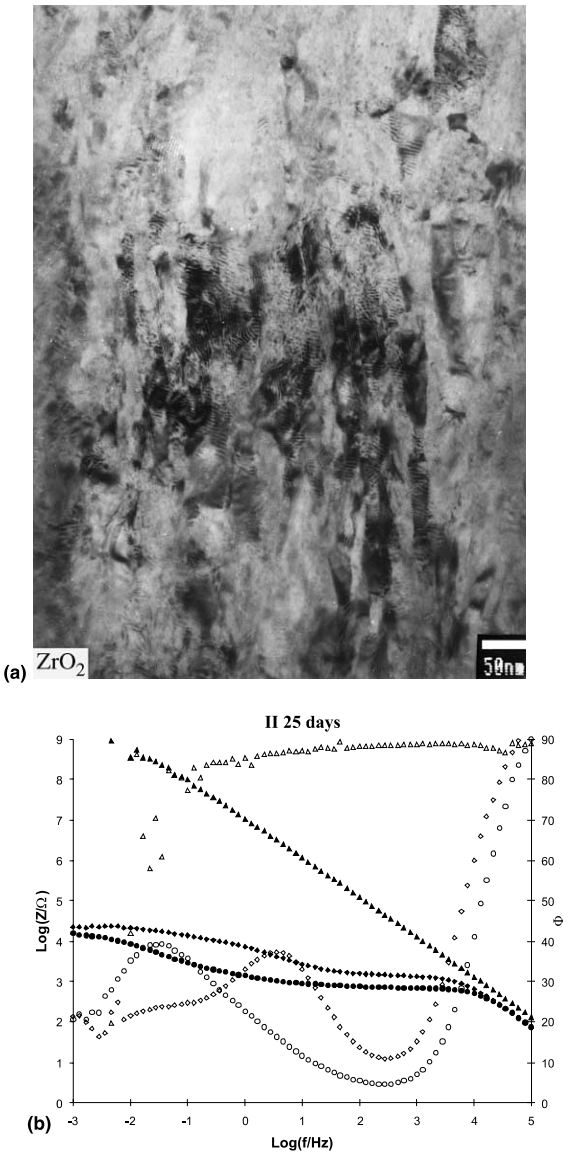

Fig. 8. Sample II after 25 days: (a) TEM micrograph; (b) EIS. Measurements in mercury (■) magnitude and (□) phase angle. Measurements in 0.5 M Na_2SO_4 at two different immersion times (●) magnitude and (○) phase angle.

3.4. SIMS

The pre-hydriding process gave, besides the bulk hydrides, a dense surface hydride layer, which was observed as a few tens μm thick layer with LOM for the 500 ppm sample (III), Fig. 1. However, this was hardly seen for the 200 ppm sample (I). With SIMS the massive hydride layer was clearly observed for the 500 ppm sample. Also for the 200 ppm sample a thin hydride layer was observed, Fig. 9(a), in agreement with XRD. The effect of the heat treatment was also very clearly seen in the SIMS depth profiling, see Fig. 9(a). The decreasing hydrogen peak at the surface, present in some samples, is not significant for the hydrogen content but is rather an effect from H-species adsorbed on the surface and in pores [13,14,26].

For the oxidised samples both the oxygen and hydrogen penetration profiles were recorded together with the hydrogen penetration profile for the non-oxidised samples. The position of the metal–oxide interface was identified at the location where the oxygen intensity has dropped by a factor of 2. The oxygen penetration profile shows a rather sharp decrease at the interface, indicating that the oxidation front is rather even, in agreement with the TEM observations. The oxygen level was not quantified and those profiles only show the relative ratio between oxygen and zirconium.

The SIMS-profiles for hydrogen in the REF specimen before and after oxidation for 10 days, are shown in Fig. 9(b). In the oxidised sample the hydrogen concentration in the oxide has a minimum value of 10 ppm (detection limit) close to the oxide/metal interface and increases approaching the outer oxide surface.

In Fig. 10(a)–(c), the SIMS-profiles for hydrogen in the 200 ppm hydrogen sample are shown, together with the profile on the corresponding non-oxidised sample. For the non-oxidised sample high levels of hydrogen are observed at the surface, representing adsorbed hydrogen species. When the surface peak has decreased, a hydrogen depleted region can be observed. Further into the metal, the intensity is again increasing, reaching the 200 ppm level. Also for the oxidised samples high levels of hydrogen can be observed at the outer oxide surface. The amount of hydrogen at the surface is higher after 10 days than after 3 days of oxidation. However, in both cases only very low levels are observed in the bulk oxide. Only for the 25 days sample there is an indication of hydrogen penetrating further into the oxide, indicating a more porous structure of the oxide. Irrespective of the

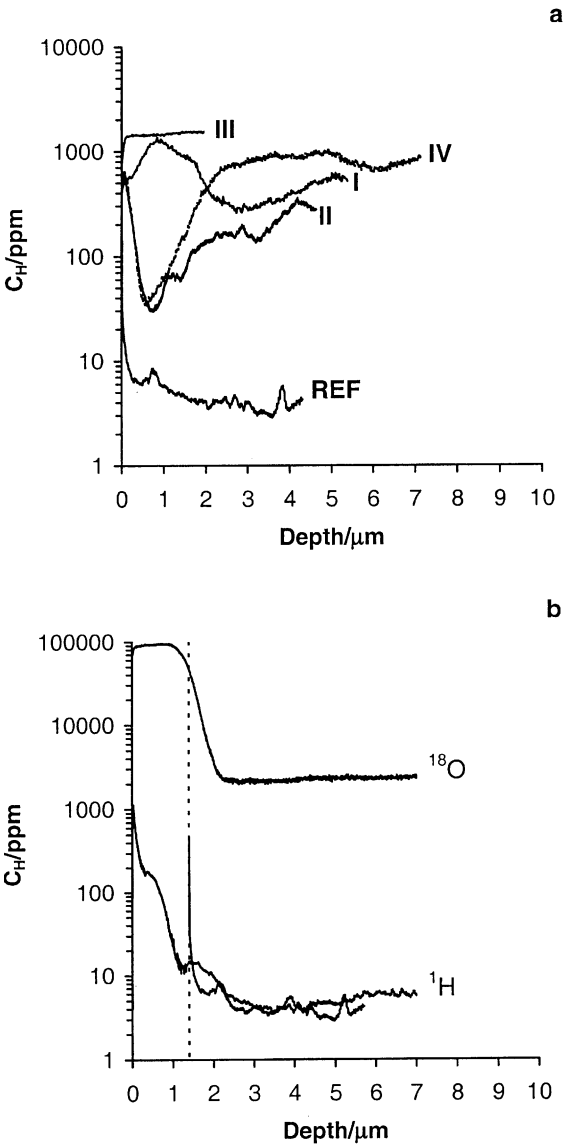

Fig. 9. (a) SIMS profiles showing the hydrogen distribution of pre-hydrided samples before (I and III) and after (II and IV) heat treatment. (b) SIMS profiles of hydrogen and oxygen distributions in the reference sample before and after oxidation at 400°C for 10 days. The hydrogen profile for the non-oxidised sample has been shifted to the position of the metal/oxide interface.

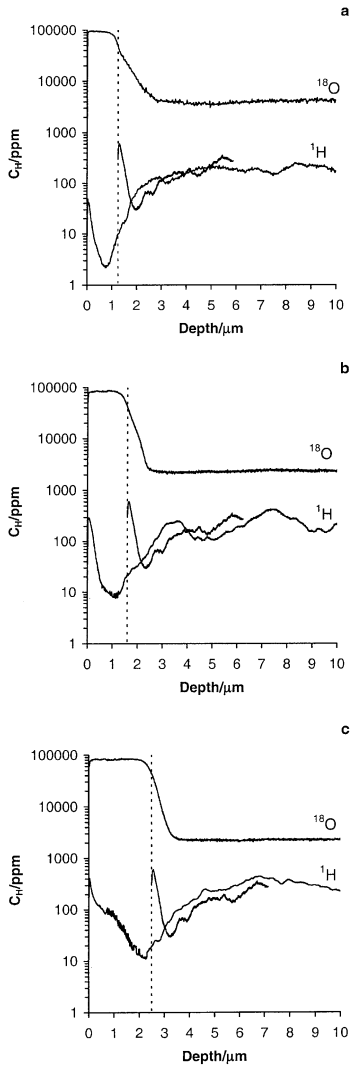

Fig. 10. SIMS profiles of hydrogen and oxygen distributions in the 200 ppm hydrided (II) sample before and after oxidation at 400°C for: (a) 3 days; (b) 10 days; (c) 25 days. The hydrogen profile for the non-oxidised sample has been shifted to the position of the metal/oxide interface.

oxidation time, the hydrogen profile in the metal remains the same as profile in the non-oxidised samples.

The fact that the hydrogen profile in the oxide reaches its lowest value somewhat before the interface, is an effect of the quantification routine where the H intensity is divided by the Zr intensity. As the Zr intensity decreases, while the H intensity is still constant, the deduced concentration starts to increase. The constant region is probably the noise background of the instrument, in which case the hydrogen concentration at the interface could be even lower in reality. Due to the changes in sputter rate and ionisation yield when passing from oxide to metal, the error in quantification is higher for this interface region. The measured oxide thickness as deduced from SIMS craters are in accordance to previous measurements, Table 2.

The SIMS-profiles for the oxidised (10 days) 500 ppm hydrogen samples (III and IV), are shown in Fig. 11, together with the corresponding profiles for the non-oxidised sample. For the sample with a massive surface

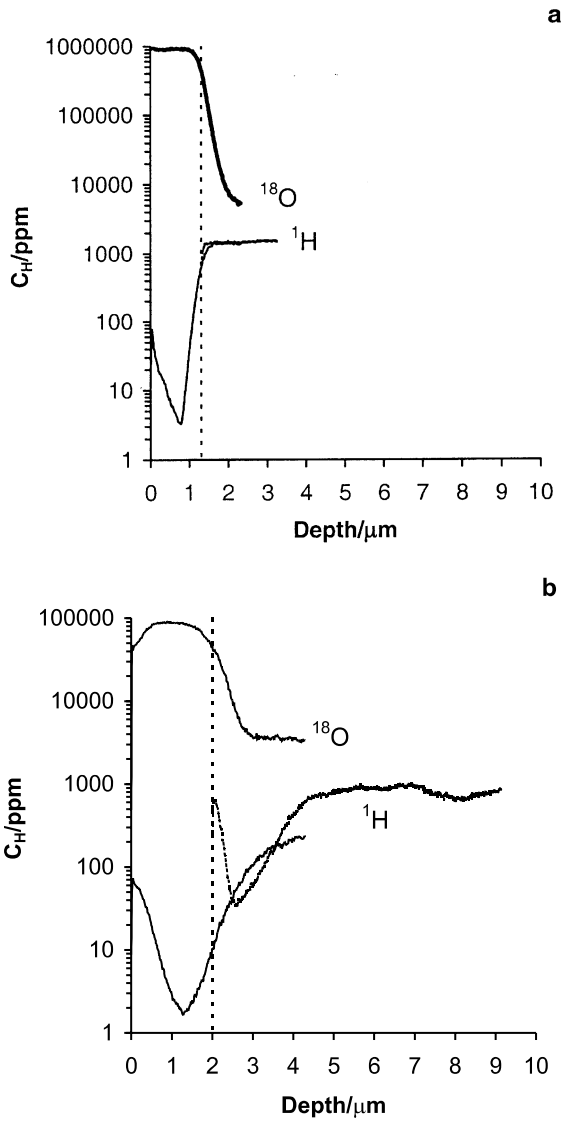

Fig. 11. SIMS profiles of hydrogen and oxygen distributions in the 500 ppm samples, before and after oxidation at 400°C for 10 days: (a) with surface hydride (III); (b) without surface hydride (IV). The hydrogen profile for the non-oxidised sample has been shifted to the position of the metal/oxide interface.

hydride (III), very high hydrogen concentrations were observed in a region that penetrate at least 20–30 μm, according to the LOM observations, Fig. 1. This made it impossible to penetrate the total hydride layer with SIMS in-depth profiling. It is interesting to note that the hydrogen level is low in the entire oxide, even for this sample with a thick massive surface hydride. For the sample with a homogeneous distribution of hydrides, the hydrogen profile in the metal is similar to the original profile of the non-oxidised sample as shown in Fig. 11(b).

The results show the great importance of a careful examination of each sample with SIMS before each processing stage. Without the knowledge about the original profile of hydrogen in these samples before autoclave experiments, it can be more difficult to make conclusions about the hydrogen migration process. Although the oxidation process proceeds inwards, it is observed that the hydrogen distribution on the metal side of the interface is very similar to the profile in the non-oxidised sample, indicating that hydrogen moves in front of the oxide/metal interface. This is probably due to the slow transport of H in the oxide as compared to the metal [5] and also expected from thermodynamic considerations.

4. Discussion

The accelerated oxidation kinetics for Zircaloy is often associated with the formation of a massive hydride layer at the metal/oxide interface [18,19,21,27]. Provided that it is the massive hydride that increases the oxidation rate it should be possible to simulate this situation by studying the oxidation of massive hydride on zirconium metal. In such a study it is possible to discriminate between the specific effect of hydride and combined effects where the hydride is involved.

In this context the pre-hydrided sample may be seen as a simulation of a post-transition oxidation, but with no oxide layer present. However, one important difference between these situations is the lack of surface roughness of the pre-hydrided sample. Samples subjected to longer corrosion tests are normally characterised by an interfacial roughness. An example of the interfacial roughness is shown by the so-called cauliflower structure of the formed oxide at the metal/oxide interface [28]. The curvature of the interface influences the compressive stresses present in the oxide. Recent theoretical calculations have shown that the geometry of the interface is important for the local stress distribution [29]. A convex curvature of the interface is associated with a greater compressive stress in the oxide than for a concave curvature. The 2D modelling of the interface undulation [29] showed the presence of a tensile stress in radial direction at the metal/oxide interface, for the convex areas (see [29, Fig. 13]). The level of the radial stress was found to be several hundred MPa and was suggested to cause cracks in the oxide near the convex areas. If cracks are formed at the interface the growth of the oxide grains will be disturbed. Further, the curvature at the interface will also influence the oxidation rate, since the driving force for oxidation is lower when higher compressive stress is present. Thus, during post-transition oxidation when the metal surface is rougher, the

hydrides may have a negative influence on the protective oxide layer by changing the stress distribution at the metal/oxide interface. It is also well known that hydrides degrade the mechanical properties of Zircaloy. When hydrides precipitate in the metal, the orientation will tend to be such that the volume increase is absorbed in the thickness direction of the metal. The oxide grown on these hydrides will therefore have a lower compressive stress compared to an oxide grown on zirconium metal and the oxidation resistance provided by the compressive stress in the oxide is then lost.

In the present study gas hydrogenation was used to produce the hydrides since cathodic charging has been claimed to be a more detrimental charging process [20,21]. Gas hydrogenation has the advantage that no oxidation of the samples occurred during the pre-hydriding, but a drawback is that only samples with low hydrogen content ($\leqslant$500 ppm) can be produced without risking to damage the surface of the samples. The levels of hydrogen used in this work, 200 and 500 ppm, were chosen in order to simulate three different test conditions during oxidation: (i) Hydrogen in solid solution in the zirconium alloy, corresponding to the initial oxidation prior to precipitation of hydrides. (ii) Uniformly distributed hydrides, simulating a situation where hydrides starts to precipitate and (iii) massive surface hydride, claimed to be the main cause of accelerated oxidation.

In this study no effect on the oxidation kinetic from hydrogen/hydrides was found in the pre-transition region. The oxidation rate is independent of the composition of the matrix, i.e. pure alloy, alloy with dissolved hydrogen, an alloy/hydride mixture or a massive hydride layer. This is in accordance with earlier studies [18,20,21], taking into account the relatively short oxidation times used. The crystalline phases, morphology, element distribution and porosity of the formed oxide layers were also found to be similar. The lack of a hydrogen influence on the oxidation kinetics is also supported by oxidation tests on zirconium hydride powder in air at 300–400°C and atmospheric pressure, where it was shown that the oxidation parallels that of zirconium metal [30]. One reason for the similar oxidation kinetics of zirconium metal and zirconium hydride might be that in both cases the oxidation rate is determined by the diffusion of oxygen. This implies that also the hydride surface is initially covered by a thin oxide layer. That the oxidation of zirconium and its alloys is limited by diffusion of oxygen ions is the prevailing conception and has been experimentally verified by marker experiments [31,32] and by measuring electrical conductivity [33].

It can be concluded that accelerated oxidation of Zircaloys cannot be explained by a faster oxidation rate of zirconium hydride compared to the metal but may be due to a combination effect of hydride precipitation, and for example interfacial roughness.

5. Conclusions

The pre-transition corrosion rate of Zr-2 was measured in the presence of hydrogen/hydrides. Oxidation tests with hydrogen present in three different states were performed: (i) Hydrogen in solid solution in the zirconium alloy, corresponding to the initial oxidation prior to precipitation of hydrides. (ii) Uniformly distributed hydrides, simulating a situation where hydrides starts to precipitate and (iii) massive surface hydride, claimed to be the main cause of accelerated oxidation. However, no effect on the oxidation kinetics from hydrogen/hydrides was found in the pre-transition region, as measured by weight gain.

X-ray analysis showed that the main oxidation product on all samples was monoclinic ZrO_2 and the TEM investigations of the morphology showed mainly columnar grains in the oxide, irrespective of the hydrogen content.

SIMS penetration profiles demonstrate that the oxidation front moves the hydrogen further into the metal and that no elevated hydrogen levels in the oxide result from oxidation of a pre-hydrided sample.

The total porosity of the oxide formed on the different samples, as measured by impedance measurements in Hg, were similar and ranged from 4% to 6%. However, the open porosity seemed to be larger for the HT samples and increases with time and increasing hydrogen content. For samples with massive surface hydride the oxide layer after 10 days oxidation at 400°C shows a homogeneous behaviour with only one time constant in the impedance spectra.

Based on these results, regarding the pre-transition oxidation on pre-hydrided samples, it is concluded that the oxidation of massive zirconium hydride resembles the oxidation of zirconium metal. Thus, the accelerated oxidation often observed after long time exposure is probably due to a combined effect of hydride precipitation and interfacial roughness, and not to a faster oxidation rate of zirconium hydride.

Acknowledgements

Financial support from the Swedish Nuclear Power Inspectorate (SKi) is gratefully acknowledged. This work was carried out as a part of the Swedish research programme for the understanding of Zircaloy corrosion and hydriding mechanisms, funded by ABB Atom AB, Barsebäck Kraft AB, OKG AB, and Vattenfall. Associate professor Gunnar Hultquist is gratefully acknowledged for providing the pre-hydrided samples.

References

[1] J.J. Kearns, J. Nucl. Mater. 22 (1967) 292.
[2] A. McMinn, E.C. Darby, J.S. Schofield, in: G.P. Sabol, G.D. Moan (Eds.), Zirconium in the Nuclear Industry: 12th International Symposium, vol. ASTM STP 1354, Toronto, Canada, 2000, p. 173.
[3] C. Roy, J. Nucl. Mater. 13 (1964) 275.
[4] S. Yamanaka, T. Tanaka, M. Miyake, J. Nucl. Mater. 167 (1989) 231.
[5] A. Stern, D. Khatamian, T. Laursen, G.C. Weatherly, J.M. Perz, J. Nucl. Mater. 148 (1987) 257.
[6] M. Miyake, M. Uno, S. Yamanaka, J. Nucl. Mater. 270 (1999) 233.
[7] W.E. Berry, D.A. Vaughan, E.L. White, Corrosion (1961) 109.
[8] J.N. Wanklyn, D.R. Silvester, J. Dalton, N.J.M. Wilkins, The corrosion of zirconium and its alloys in high temperature steam. Part II. The uptake of hydrogen during corrosion, UKAEA Report AERE-R3768, 1961.
[9] E. Hillner, Hydrogen absorption in Zircaloy-2 during aqueous corrosion: effect of environment. Report WAPD-TM-411, 1964.
[10] T. Smith, J. Nucl. Mater. 18 (1966) 323.
[11] B. Cox, The oxidation and corrosion of zirconium and its alloys. Part. XII, Hydrogen absorption by Zircaloy-2 and some other alloys during corrosion in steam, AERE-R3556, 1961.
[12] B.D. Warr, M.B. Elmoselhi, S.B. Newcomb, N.S. McIntyre, A.M. Brennenstuhl, P.C. Lichtenberger, in: C.M. Eucken, A.M. Garde (Eds.), Zirconium in the Nuclear Industry: Ninth International Symposium, vol. ASTM STP 1132, Kobe, Japan, 1991, p. 740.
[13] B. Cox, Y.-M. Wong, J. Nucl. Mater. 270 (1999) 134.
[14] B. Cox, J. Nucl. Mater. 264 (1999) 283.
[15] B. Cox, Atomic Energy of Canada Ltd., vol. AECL-8702, 1985.
[16] Y. Hatano, K. Isobe, R. Hitaka, M. Sugisaki, J. Nucl. Sci. Technol. 33 (1996) 944.
[17] Y. Hatano, R. Hitaka, M. Sugisaki, M. Hayashi, J. Nucl. Mater. 248 (1997) 311.
[18] T. Kido, in: R.E. Gold, E.P. Simonen (Eds.), Sixth International Symposium on Environmental Degradation of Materials in Nuclear Power System – Water Reactors, San Diego, CA, USA, 1993, p. MMMS 449.
[19] A.M. Garde, in: C.M. Eucken, A.M. Garde (Eds.), Zirconium in the Nuclear Industry: Ninth International Symposium, vol. ASTM STP 1132, Kobe, Japan, 1991, p. 566.
[20] M. Blat, D. Noel, in: E.R. Bradley, G.P. Sabol (Eds.), Zirconium in the Nuclear Industry: 11th International Symposium, vol. ASTM STP 1295, Garmisch-Partenkirchen, Germany, 1996, p. 319.
[21] M. Blat, L. Legras, D. Noel, H. Amanrich, in: G.P. Sabol, G.D. Moan (Eds.), Zirconium in the Nuclear Industry: 12th International Symposium, vol. ASTM STP 1354, Toronto, Canada, 2000, p. 563.
[22] F. Garzarolli, H. Seidel, R. Tricot, J.P. Gros, in: C.M. Eucken, A.M. Garde (Eds.), Zirconium in the Nuclear Industry: Ninth International Symposium, vol. ASTM STP 1132, Kobe, Japan, 1991, p. 395.
[23] B. Wadman, Z. Lai, H.-O. Andren, A.-L. Nyström, P. Rudling, H. Pettersson, in: A.M. Garde, E.R. Bradley (Eds.), Zirconium in the Nuclear Industry: 10th International Symposium, vol. ASTM STP 1245, Baltimore, MD, 1994, p. 579.
[24] P. Meisterjahn, H.W. Hoppe, J.W. Schultze, J. Electroanal. Chem. 217 (1987) 159.
[25] E.M. Patrito, R.M. Torresi, E.P.M. Leiva, V.A. Macagno, J. Electrochem. Soc. 137 (1990) 524.
[26] U. Södervall, E. Ahlberg, in: ECASIA 97 proceedings of the European Conference on Applications of Surface and Interface Analysis, Göteborg, Sweden, 1997, p. 389.
[27] Y.S. Kim, K.S. Rheem, D.K. Min, in: A.M. Garde, E.R. Bradley (Eds.), Zirconium in the Nuclear Industry: 10th International Symposium, vol. ASTM STP 1245, Baltimore, MD, 1994, p. 745.
[28] G. Wikmark, P. Rudling, B. Lehtinen, B. Hutchinson, A. Oscarsson, E. Ahlberg, in: E.R. Bradley, G.P. Sabol (Eds.), Zirconium in the Nuclear Industry: 11th International Symposium, ASTM STP 1295, American Society for Testing and Materials, Garmisch-Partenkirchen, 1996, p. 55.
[29] M. Parise, O. Sicardy, G. Cailletaud, J. Nucl. Mater. 256 (1998) 35.
[30] V.Z. Shemet, V.A. Lavrenko, O.A. Teplov, V.Z. Ratushnaya, Oxid. Met. 38 (1992) 8998.
[31] B. Cox, C. Roy, Electrochem. Techn. 4 (1966) 121.
[32] A. Grandjean, Y. Serruys, J. Nucl. Mater. 273 (1999) 111.
[33] M.M.R. Howlader, K. Shiiyama, C. Kinoshita, M. Kutsuwada, M. Inagaki, J. Nucl. Mater. 253 (1998) 149.